



Dinickel enzyme evolved to metabolize the pharmaceutical metformin and its implications for wastewater and human microbiomes

Lambros J. Tassoulas^{a,b}, Joel A. Rankin^{a,b}, Mikael H. Elias^{a,b}, and Lawrence P. Wackett^{a,b,1}

Edited by Amy Rosenzweig, Northwestern University, Evanston, IL; received July 24, 2023; accepted January 12, 2024

Metformin is the first-line treatment for type II diabetes patients and a pervasive pollutant with more than 180 million kg ingested globally and entering wastewater. The drug's direct mode of action is currently unknown but is linked to effects on gut microbiomes and may involve specific gut microbial reactions to the drug. In wastewater treatment plants, metformin is known to be transformed by microbes to guanylurea, although genes encoding this metabolism had not been elucidated. In the present study, we revealed the function of two genes responsible for metformin decomposition (mfmA and mfmB) found in isolated bacteria from activated sludge. MfmA and MfmB form an active heterocomplex (MfmAB) and are members of the ureohydrolase protein superfamily with binuclear metal-dependent activity. MfmAB is nickel-dependent and catalyzes the hydrolysis of metformin to dimethylamine and guanylurea with a catalytic efficiency $(\dot{k}_{cat}/\dot{K_M})$ of 9.6×10^3 M⁻¹s⁻¹ and K_M for metformin of 0.82 mM. MfmAB shows preferential activity for metformin, being able to discriminate other close substrates by several orders of magnitude. Crystal structures of MfmAB show coordination of binuclear nickel bound in the active site of the MfmA subunit but not MfmB subunits, indicating that MfmA is the active site for the MfmAB complex. Mutagenesis of residues conserved in the MfmA active site revealed those critical to metformin hydrolase activity and its small substrate binding pocket allowed for modeling of bound metformin. This study characterizes the products of the mfmAB genes identified in wastewater treatment plants on three continents, suggesting that metformin hydrolase is widespread globally in wastewater.

metformin | biodegradation | human gut microbiome | metallohydrolase | nickel

Metformin is the first-line therapeutic drug for type II diabetes and one of the most prescribed drugs in the world with over 250 million daily prescriptions. The large daily dose of 1 to 2 g, when ingested by patients, is not metabolized in the liver and is eliminated in urine and feces, entering wastewater. This amounts to more than 100 million kg of metformin entering the environment each year and is nearly as pervasive as caffeine in global waters (1, 2). In addition, metformin has been identified, more recently, to have antiobesity, antiaging, and antitumor properties, and the future use of this drug could be extended beyond type II diabetes (3). The mechanism of action for metformin has been under intense scrutiny for the past couple of decades, but a direct mode of action is still unclear. Recent studies point to metformin's interaction with human gut microbes for exerting therapeutic effects (4–7). A study involving intravenous administration of metformin to type II diabetes patients, that mainly bypasses the human gut, showed little to no efficacy (8).

Human gut microbes are important in regulating human health, and they are also known to modulate drug potency and side effects by gut drug metabolism in several cases (9-11). Studies that track the disposition of metformin show complete recovery of metformin after intravenous administration but incomplete recovery (~80%) after oral dosage (12, 13). This possibly may be due to partial, gut-drug metabolism, although a metastudy concluded that metformin metabolism in humans is still equivocal (14). There is evidence for metformin metabolism to guanylurea in rats (15). Identifying genes and enzymes that mediate metformin metabolism could give insight into what metabolites are possibly generated and the genes involved in the gut.

Microbial metabolism of metformin is known in wastewater treatment plants (WWTPs), with some reports finding significant transformation (>80%) (16–18). The transformation is known to occur due to microbes in the activated sludge of WWTPs, with guanylurea found to be the main transformation product (16, 19, 20). Chronic exposure of environmentally relevant concentrations of metformin and guanylurea is known to be toxic to zebrafish, affecting reproduction, larvae survival, and neurobehavior (21, 22). Other water treatment methods to remove metformin have proven to be ineffective as metformin has

Significance

Metformin is a pervasive pollutant and the first-line treatment for type II diabetes with a mechanism of action that remains elusive. Recent findings point to the drug's interaction with human gut microbes to exert the therapeutic effect. In wastewater treatment plants (WWTPs), metformin is metabolized by microbes. Herein, we characterize a metaldependent metformin hydrolase found in bacteria from activated sludge of WWTPs across three continents. We determined the enzyme kinetic parameters, substrate specificity, X-ray structure and find the enzyme to be specialized in metformin hydrolysis. The elucidation of the genes encoding metformin degradation may aid future mechanistic research of metformin and possibly be used to augment wastewater treatment capabilities in the future.

Author affiliations: aDepartment of Biochemistry, Biophysics, and Molecular Biology, University of Minnesota, Minneapolis, MN 55455; and ^bBioTechnology Institute, University of Minnesota, St. Paul, MN 55108

Author contributions: L.J.T., J.A.R., M.H.E., and L.P.W. designed research; L.J.T. and J.A.R. performed research; L.J.T., J.A.R., M.H.E., and L.P.W. analyzed data; and L.J.T., M.H.E., and L.P.W. wrote the paper.

The authors declare no competing interest.

This article is a PNAS Direct Submission.

Copyright © 2024 the Author(s). Published by PNAS. This article is distributed under Creative Commons Attribution-NonCommercial-NoDerivatives License 4.0

¹To whom correspondence may be addressed. Email: wacke003@umn.edu.

This article contains supporting information online at https://www.pnas.org/lookup/suppl/doi:10.1073/pnas. 2312652121/-/DCSupplemental.

Published February 26, 2024

poor affinity with activated carbon and chlorination of metformin creates N-chloro species that have been shown to be toxic to human cells (23-25). Thus, biodegradation of metformin by activated sludge microbes is seen as a viable strategy for its removal, although the enzyme initiating its metabolism had previously not been studied.

In recent years, several microbes have been isolated from activated sludge that can utilize metformin as a carbon or nitrogen source for growth, and their genomes have been sequenced (26–30). Aminobacter isolates have been shown to break down metformin, utilizing the dimethylamine fragment and exporting guanylurea via a drug transporter (27, 28). We reported on the isolation of a Pseudomonas species that could utilize guanylurea as the sole nitrogen source and identified a guanlyurea hydrolase (GuuH) that deaminates guanylurea to form guanidine (31). The same species also possessed the genes to break down guanidine completely via guanidine carboxylase, carboxyguanidine deiminase (CgdAB), and allophanate hydrolase (32). More recently, we reported on another Pseudomonas species isolate that could mineralize metformin completely and three independent studies describe metformin-degrading Aminobacter strains (27-29). Comparative genomics with those bacteria revealed two contiguous genes (mfmA and mfmB) that encoded proteins for which substrate specificity data were lacking.

Here, we report that these two genes, *mfmA* and *mfmB*, encode a metal-dependent metformin hydrolase (MfmAB) and characterize its kinetics, substrate specificity, and X-ray structure and find the genes to be widespread globally in wastewater treatment plants and perhaps in human gut microbiomes.

Results

Identification of a Metformin Hydrolase, MfmAB, That Hydrolyzes Metformin to Guanylurea and Dimethylamine. The metformin hydrolase genes, mfmA and mfmB, tested in this study came from Pseudomonas mendocina sp. MET-2, isolated from activated sludge of the Metropolitan Wastewater Treatment Plant in Saint Paul, Minnesota, United States (27). Metformin hydrolase, MfmAB, is a complex of MfmA and MfmB proteins that are homologous to each other (34% sequence identity, seq. id.) and related to proteins from the ureohydrolase superfamily (Fig. 1). The MfmAB genes appear, putatively, in an operon with putative nickel delivery proteins (HypB and HypA), a putative nickel importer (UreJ), and a putative metformin transporter (CodB) (Fig. 1A). The MfmAB operon is also present and highly conserved (>97% amino acid seq. id.) in five other *Pseudomonas* and *Aminobacter* species that can grow on metformin and isolated from activated sludge across three continents (SI Appendix, Fig. S1). The Pseudomonas strains have been characterized to utilize metformin as a sole nitrogen source (27, 30) while the Aminobacter strains can utilize metformin as a carbon and nitrogen source (28, 29). The heterologous expression of MfmA or MfmB individually in Escherichia coli showed no activity on metformin in lysates. Only when the two proteins were coexpressed was activity present, as determined by a decrease in metformin and concomitant appearance of guanylurea via HPLC (Fig. 1B). In expression studies, MfmA does not produce soluble protein when expressed singly although individually expressed MfmB produces soluble protein (SI Appendix, Fig. S2A). Repeated attempts to obtain soluble MfmA protein were not successful. Thus, the strategy developed to purify the MfmAB complex was fusing MfmA to a C-terminal 6×His-tag, allowing the copurification of MfmB with MfmA. Two bands of protein were seen on a denaturing polyacrylamide gel at ~41 kDa and 38 kDa corresponding to His-tagged MfmA and MfmB, respectively

(Fig. 1C). The protein gel band for MfmB was consistently denser than the band for MfmA, suggesting that the stoichiometry of the heterotrimer is 2:1 MfmB:MfmA. By gel filtration, the purified complex elutes with an apparent molecular weight of 179 ± 3 kDa (n = 3) compared to a series of standards (SI Appendix, Fig. S13). This is considerably larger than the calculated mass of the heterotrimer of 117 kDa. Based on the crystallization model (vide infra), we conclude that the heterotrimer is the authentic structure in solution. We suspect that the complex has a larger hydrodynamic volume than its size would suggest due to two axes being longer than the third. The effect of hydrodynamic volume on apparent molecular weight of proteins has been previously noted (33). It was demonstrated that MfmAB could transform metformin to guanylurea, suggesting that dimethylamine was the second product of the reaction. Using ¹H NMR, the transformation of metformin with MfmAB was monitored by following the chemical shift of the methyl hydrogens on the dimethylamine moiety (Fig. 1D). This chemical shift moved upfield, from 3.06 to 2.73 ppm, upon adding MfmAB to metformin, the latter chemical shift was identical to a dimethylamine standard (SI Appendix, Fig. S3).

MfmA and MfmB are both homologous to known enzymes such as arginase, agmatinase, and guanidinium hydrolase of the ureohydrolase protein superfamily (InterPro IPR006035) that possess a binuclear metal binding site and catalyze the hydrolysis of guanidinium groups to form urea and an amine (Fig. 1*E*) (34, 35). A multiple sequence alignment of the sequences of MfmA and MfmB with arginase and agmatinase highlighted the conserved residues, present in MfmA but not MfmB, that coordinate the binuclear metal ions in arginase and agmatinase enzymes (Fig. 1*E*).

MfmAB Is a Nickel-Dependent Metallohydrolase with Exquisite Substrate Specificity. The pH optimum of MfmAB was sharp between pH 9 and 9.5 (Fig. 2A). The alkaline pH optimum is characteristic of enzymes in the ureohydrolase protein superfamily like arginase and agmatinase as it is proposed that the nucleophile is a metal-bound hydroxide in the hydrolysis reaction (36, 37). MfmAB was not fully active in the absence of certain divalent metals. When MfmAB was stripped of metals and then reconstituted with divalent metals, nickel showed the highest activation, with cobalt and manganese having less activity and iron showing activity comparable to the no metal control (Fig. 2B). When MfmAB was coincubated with nickel and copper or zinc, no guanylurea formation was detected by HPLC. Analysis of the metal content of purified MfmAB by inductively coupled plasma-optical emission spectroscopy (ICP-OES) showed substoichiometric amounts of zinc, nickel, and iron. Nickel activated MfmAB to the greatest extent and genes colocated with *mfmA* and *mfmB* in genomes are annotated as encoding nickel delivery and transport proteins (Fig. 1A and SI Appendix, Fig. S1) (27, 28). In light of this, nickel was chosen to activate MfmAB in all subsequent enzyme kinetic experiments.

To characterize the enzyme kinetics of MfmAB, a spectrophotometric, coupled-enzyme assay included the enzymes guanylurea hydrolase (GuuH) and glutamate dehydrogenase (GDH) in admixture with MfmAB to measure NADH oxidation that was proportional to guanylurea release from MfmAB (SI Appendix, Fig. S5). Guanylurea is released from the MfmAB reaction with metformin and biguanide analogs and guanylurea hydrolysis, via GuuH, generates guanidinium and ammonia. The latter can be used in reductive amination of 2-oxoglutarate to form L-glutamate, supporting NADH oxidation that can be measured by a decrease in absorbance at 340 nm. MfmAB was found to be very specific to metformin, with no other substrate showing more than 0.6% of the activity observed for metformin (Fig. 2C). Buformin (1-butylbiguanide) was the second most active substrate while

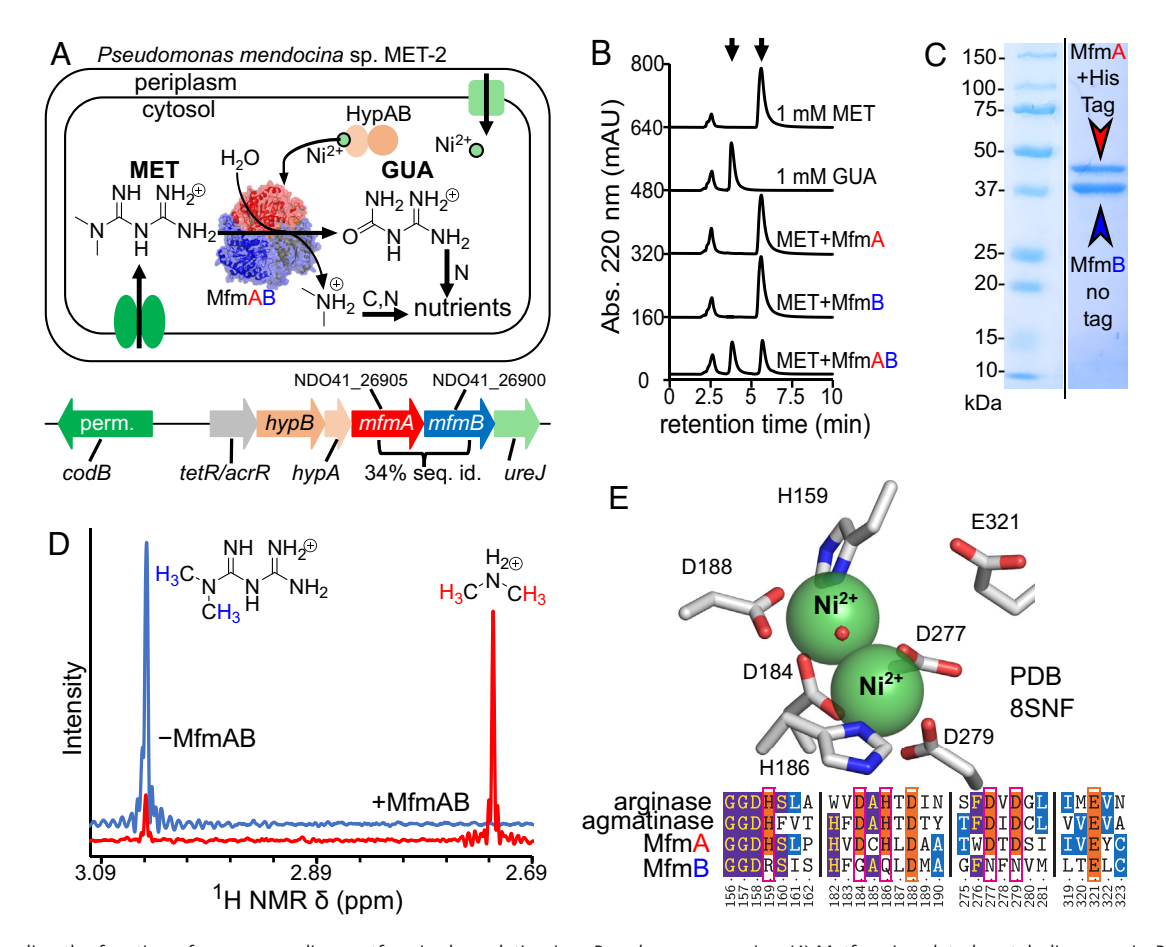


Fig. 1. Revealing the function of genes encoding metformin degradation in a Pseudomonas species. (A) Metformin-related metabolic genes in Pseudomonas mendocina sp. MET-2 are in a putative operon which encode metformin hydrolase (MfmA and MfmB), nickel metabolism proteins (HypB and HypA), a putative nickel importer (Urej), and a putative metformin transporter (CodB). MfmA and MfmB are both homologs of the ureohydrolase superfamily and share 34% sequence identity to each other. The Pseudomonas species has additional genes to completely mineralize guanylurea as a nitrogen source and utilize dimethylamine as a source of carbon or nitrogen. NCBI Genbank identifiers for the mfmA and mfmB genes are shown above the genes in the putative operon. (B) Activity on metformin was found only in E. coli lysates when MfmA and MfmB were coexpressed (MfmAB) and not individually. Lysates were incubated with 1 mM metformin for 1 h in 20 mM CHES pH 9 with 1 mM NiCl₂ before being sampled using an HPLC method that can separate guanylurea from metformin. Guanylurea was identified as $the\ reaction\ product\ of\ MfmAB.\ (\emph{C})\ MfmB\ copurifies\ with\ His-tagged\ MfmA.\ Stained,\ denaturing,\ polyacrylamide\ gel\ with\ purified\ MfmAB\ after\ IMAC.\ A\ band\ was$ observed for 6×His-tagged MfmA and a more intense band was seen for MfmB despite not being tagged. See SI Appendix, Fig. S2 for the full gel. (D) Identification of dimethylamine as a reaction product of MfmAB by 1H NMR. NMR spectra were obtained for 50 mM metformin in 50 mM ammonium formate, 200 mM NaCl pH 8.5, and 1 mM NiCl₂ with 20% (v/v) D₂O before (blue spectrum) and after 1-h incubation with 200 µg purified MfmAB (red spectrum). The major shift for the methyl hydrogens changed upon MfmAB addition from 3.06 ppm to 2.73 ppm which was identical to the shift found for the dimethylamine standard. See SI Appendix, Fig. S2, for full NMR spectra. (E) MfmA and MfmB are homologous to arginase and agmatinase with binuclear divalent metal centers, yet MfmB has lost several key metal binding residues. The active site of MfmA is shown with the binuclear metal center and the several histidine and aspartate residues binding it. A multiple sequence alignment showing sequence conservation shared between human arginase I (PDB 2AEB), E. coli agmatinase (PDB 7LOL), MfmA, and MfmB is depicted. Numbering of amino acids is based on the sequence of MfmA.

other biguanides such as phenformin (1-phenylethylbiguanide), 1-methylbiguanide, and biguanide were much less reactive. Of the different guanidines tested, dimethylguanidine had similar activity to buformin, with methylguanidine having less activity (*SI Appendix*, Table S1).

Michaelis–Menten kinetics were determined for the cleaved His-tag MfmAB with a K_M of 0.82 mM and a catalytic efficiency (k_{cat}/K_M) of 9.6 × 10³ M⁻¹ s⁻¹ at the pH optimum (pH 9). At pH 8, the catalytic efficiency of MfmAB decreased to 8.7 × 10² M⁻¹s⁻¹ and the K_M increased to 6.1 mM (Fig. 2*D*). The cleavage of the His-tag led to an activity increase of ~25%, but the K_M was not affected (*SI Appendix*, Table S2). The activity of the enzyme was temperature dependent, with thermal inactivation of the enzyme seen at 65 °C (*SI Appendix*, Fig. S4*A*). The activation energy for metformin hydrolysis by MfmAB at pH 8 was estimated from an Arrhenius plot to be 52.9 kJ mol⁻¹ (*SI Appendix*, Fig. S4*B*). This value was comparable to the activation energy for enzymatic hydrolysis of guanidine catalyzed by GdmH reported to be 56.1 kJ mol⁻¹ at pH 8 (34). Both metformin and guanidine

are resonance-stabilized molecules, and it is estimated that GdmH accelerates guanidine hydrolysis, over the spontaneous rate, on the order of 10¹³, similar to arginase and agmatinase of the ureohydrolase protein superfamily (34, 38).

Crystal Structure of MfmAB. Diffraction data for crystals of MfmAB were collected at resolution ranging from 1.85 to 2.30Å. The structure was solved by molecular replacement using, as template, separate AlphaFold models for MfmA and MfmB, respectively (SI Appendix, Table S3) (34). MfmAB was found to crystallize with multiple asymmetric unit sets of parameters in space group P1 and in space group C2. The oligomeric state of MfmAB observed in the crystal structures was heterotrimeric with a stoichiometry of 2:1 MfmB:MfmA (Fig. 3A). Both MfmA and MfmB subunits exhibit the arginase α/β fold characteristic of the ureohydrolase superfamily, with eight parallel β -sheets and alternating α -helices (39, 40). Also characteristic of this protein superfamily is the cis-peptide bonds present in MfmA (G156-G157) and MfmB (G135-G136). Similar to guanidine

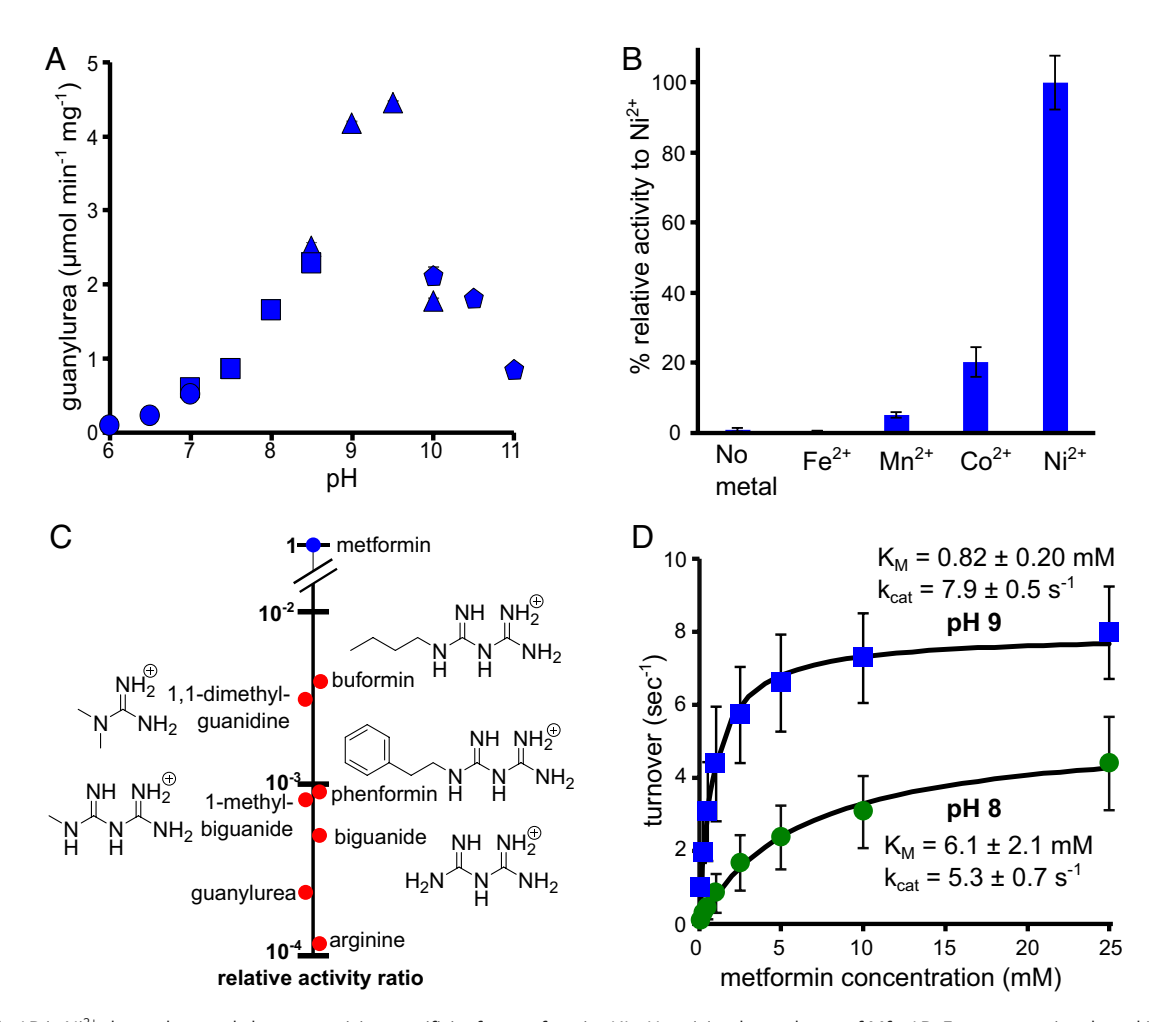


Fig. 2. MfmAB is Ni²⁺-dependent and shows exquisite specificity for metformin. (*A*) pH-activity dependence of MfmAB. Enzyme was incubated in different pH buffers for 15 min before adding 15 mM metformin and sampling after another 15 min. The pH buffer types used, 50 mM, were PIPES (pH 6 to 7, shown as circles), HEPES (pH 7 to 8.5, squares), CHES (pH 8.5 to 10, triangles), and CAPS (pH 10 to 11, pentagons). Error bars denote one SD of the mean from averaging two technical replicates. (*B*) Metal-activity dependence of MfmAB. Enzyme, stripped of metal, was reconstituted with or without 0.1 mM of several divalent metals, and activity was measured by a coupled-enzyme assay in 50 mM CHES pH 9 with 5 mM metformin. Error bars denote one SD of the mean from two technical replicates. (*C*) Plot of specificity ratios of MfmAB activity for various substrates relative to metformin. No other substrate tested showed activity more than 1% than that of metformin. Specific activities were measured by incubating purified MfmAB with 50 mM substrate in 100 mM CHES pH 9 buffer using a coupled-enzyme assay with two technical replicates. (*D*) Michaelis-Menten kinetics of metformin hydrolase at pH 9 (squares) and pH 8 (circles). Activity at several metformin concentrations was measured by observing guanylurea release using a coupled-enzyme assay in either 50 mM CHES pH 9 or 50 mM HEPES pH 8 buffer. Error bars denote one SD of the mean from three biological replicates. Black lines show the fit to the Michaelis-Menten equation.

hydrolase (GdmH), MfmA and MfmB have N-terminal loops of approximately 60 and 45 amino acids, respectively, that are not commonly found in the arginase fold and lie at the intersubunit interfaces of MfmAB (Fig. 3B) (34). Residues 16 to 24 comprise an N-terminal loop of MfmB that was highly disordered and could not be resolved from the electron density maps. When nickel was cocrystallized with MfmAB, anomalous dispersion difference maps at the K-edge for nickel identified its presence at the canonical binuclear metal binding site of MfmA subunits but not of MfmB (Fig. 3C). The active site of MfmAB resided totally within the MfmA subunits. The MfmB subunit may occlude the entrance to the active site of MfmA, but no residues of MfmB come within 10 Å of the metals bound in MfmA. No conformational differences were observed for MfmA and MfmB between the crystal structures, despite the multiple, distinct asymmetric units found.

The canonical binuclear binding site in MfmA is formed by four aspartate residues (D184, D188, D277, and D279) and two histidine residues (H159 and H186) (Figs. 1*E* and 3*C*). The active site also includes a key glutamate residue E321 which is implicated in substrate binding for agmatinase and arginase (Fig. 3*D*). The aforementioned residues correspond to critical activity determining residues

that were subject to mutagenesis in arginase and agmatinase homologs in prior studies (37, 41, 42). To expand the scope of residues critical for metformin hydrolysis, select residues in the active site, that were shown to be only conserved in close MfmA homologs (>60% seq. identity), were singly substituted, and specific activity was measured (*SI Appendix*, Fig. S6). These residues were Q81, D188, N200, C201, and W232. All substitutions were deleterious, with the variants D188N and N200A having 0.05% and 5.6% of the activity relative to the wild type. The MfmA/D188N variant was crystallized (PDB 8SNK), and it showed occupancy for only one of the two metal binding sites in the active site (*SI Appendix*, Fig. S7).

Cocrystallization of MfmAB with metformin and other compounds was unsuccessful in achieving substrate- or ligand-bound structures. Computational docking of metformin into the MfmA active site was done to model the potential catalytic conformation (Fig. 3D). A docking model positioned metformin such that the carbon atom bonded to the dimethylamine leaving group is close (2.1 Å) to the critical, attacking water molecule that is bound by the metal ions. In addition, two of the amino groups of metformin are positioned near the two metal ions at less than 2.7 Å. In this hypothetical conformation, residues N200 and E321 could provide

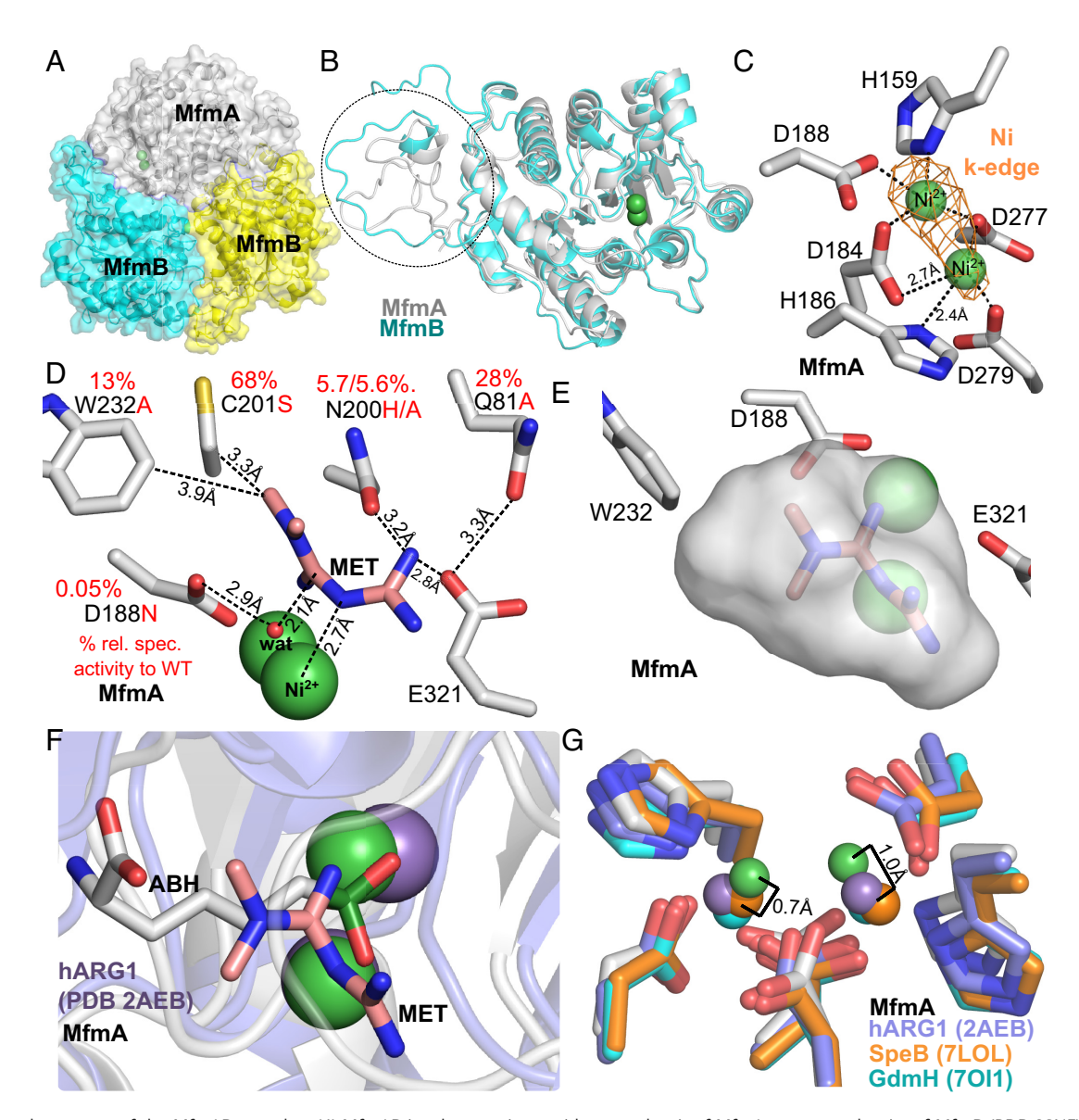


Fig. 3. Crystal structure of the MfmAB complex. (*A*) MfmAB is a heterotrimer with one subunit of MfmA per two subunits of MfmB (PDB 8SNF). (*B*) Overlay of MfmA and MfmB subunits shows high structural conservation apart from their N-terminal loops which provide contacts at the intersubunit interfaces of MfmAB (PDB 8SNF). (*C*) Active site of MfmA showing the anomalous dispersion difference maps contoured at 4σ found from diffraction data collected at the Ni edge, 8,347 eV, shown in orange mesh. Data were also collected under the Ni K-edge (8,250 eV), but the map (red mesh) shows no density peak at this contour level (PDB 8SNF). (*D*) Docking model of metformin bound to the active site of MfmA and mutagenesis. Select residues in the MfmA active site were substituted, singly, with the amino acids written in red next to the residue position and the relative specific activity to the WT stated above each residue tested. The residue substitution D188N was critical to activity which is implicated in activating the water that attacks the substrate. The relative activities reported are an average from two technical replicates with percent error of one SD being less than 3%. (*E*) Cavity of MfmA active site with metformin docked. (*F*) Overlay of docked metformin in MfmA with human arginase I (hARG1) bound with a boronic acid arginine analog, ABH, (PDB 2AEB). The docking model aligns well the dimethylamine moiety with the boronic acid group. (*G*) Overlay of metal centers from different ureohydrolase homologs, MfmA (PDB 8SNF), hARG1 (PDB 2AEB), *E. coli* SpeB (PDB 7LOL) and GdmH (PDB 7011). The positioning of the metals in MfmA (green), relative to the other homologs in the superfamily, may dictate substrate specificity.

hydrogen bonding interactions to the substrate while C201 and W232 may provide van der Waals (VDW) contacts to metformin. The MfmA active site cavity is small, and metformin docks snuggly in the cavity (Fig. 3*E*). Overlaying the metformin MfmA docking model with the crystal structure of human arginase I (hARG1) bound with a boronic acid analog of the substrate arginine (PDB 2AEB) showed that the dimethylamine moiety of metformin aligned with the alkyl chain of the boronic acid analog (Fig. 3*F*) (43). In addition, the metformin guanidinium atoms in the docking model are coordinating the metals similarly to the crystallized boronic acid analog.

Comparing the active sites of MfmA with the homologous enzymes arginase, agmatinase, and guanidinium hydrolase showed differences that relate to substrate selectivity. First, the positions of

the metals in MfmAB are not aligned precisely with the metals in the hARG1 structure. The metals in *E.coli* agmatinase and GdmH also show significant deviation (Fig. 3*G*). Second, MfmAB is missing a histidine residue, that is conserved in other ureohydrolase homologs and is implicated in the catalytic mechanism (37, 41). In MfmAB, the corresponding residue is an asparagine (N200) (Fig. 3*D*).

Discussion

MfmAB displays exquisite substrate specificity for metformin, being able to discriminate other close substrates by several orders of magnitude (Fig. 2*C*). In addition, MfmAB has a catalytic efficiency of approximately $10^4 \text{ M}^{-1}\text{s}^{-1}$, an order of magnitude less than the average $(10^5 \text{ M}^{-1}\text{s}^{-1})$ for enzymes active on natural

metabolites (Fig. 2D) (44). This is remarkable for an enzyme thought to have evolved recently; metformin has only been approved for pharmaceutical use since 1958. Prior to the introduction of metformin, the structurally analogous biguanides buformin and phenformin were used for treating type II diabetes but have since been discontinued in many countries due to metformin's superior safety profile (45). However, in South America and Asia, buformin and phenformin are still being prescribed, and wastewater bacteria possessing MfmAB could degrade these pharmaceuticals, albeit more slowly. Microbes able to grow on metformin have been isolated from activated sludge in China, Europe, and the United States (27-29). From those genomes, we have determined the presence of high-confidence homologs (>97% seq. id) of MfmA and MfmB, indicating that metformin hydrolase is widespread globally in wastewater (SI Appendix, Fig. S1).

Evolution of the MfmAB Complex. MfmB appears to be always colocated with MfmA in genomes, and the role of the subunit appears to serve as a scaffold to stabilize the fold of the active MfmA subunit (SI Appendix, Fig. S1). Mining for related sequences of MfmA and MfmB sequences from the NCBI and EMBL databases and clustering the data using a sequence similarity network (SSN) find only a few dozen closely related sequences (seq. id. >60%) to MfmA and MfmB in recorded databases (SI Appendix, Fig. S8). The cluster of MfmA sequences appears to be the closest relative of MfmB sequences, which suggests that an ancient gene duplication event of MfmA likely occurred to evolve MfmB (SI Appendix, Fig. S8). A similar example of this type of enzyme evolution is found in guanidine metabolism for the enzyme carboxyguanidine deiminase (CgdAB) (32). The CgdAB enzyme is comprised of two homologous proteins with one chain conserving the catalytic residues (CgdB) while the other chain (CgdA) lacks metal-binding residues but is still necessary for the activity of the enzyme (32). Examining the crystal structure of the MfmAB complex does not reveal that MfmB provides contacts for substrates bound in the MfmA active site. However, there is a highly disordered loop at the N terminus of MfmB (residues 16 to 24) that may play a role in gating of substrates into the MfmA active site (SI Appendix, Fig. S9). In addition, it may be possible that the loop is involved to bind the HypAB proteins and assist nickel loading into the active site of MfmA.

As the proteins MfmA and MfmB only share 34% sequence identity, it does not suggest that their interaction is a recent evolutionary event in response to metformin entering the environment, but the functional precursor to MfmAB is yet unknown. In a study by Chaignaud et al, several Aminobacter bacterial strains were unable to grow on metformin as the sole carbon source despite their genomes encoding a MfmA homolog that shared ~93% seq. id. with the MfmA reported here (SI Appendix, Fig. S10A) (28). It appears that fewer than 14 substitutions were necessary to evolve this protein to become active specifically on metformin as shown in the present study (SI Appendix, Fig. S10A). The substitution positions are distributed globally across the protein, although substitutions on one active site loop stand out (SI Appendix, Fig. S10). MfmA residues 289 to 291 on an active site loop may provide contacts for metformin, according to the docking model, and at these positions, the substitutions from MfmA, to homologs that putatively do not work on metformin, are N289S, S290T, and A291S. These changes appear very subtle, but these residues are proposed to be within 3.3 to 3.5Å with the substrate and could provide van der Waals interactions (SI Appendix, Fig. S11). Obtaining a crystal structure of one of these homologs that putatively do not work on metformin may reveal structural differences in the secondary structure of this loop or other parts of the protein

that may also dictate substrate specificity. The few differences between MfmA and non-metformin-degrading homologs support a recent evolution hypothesis and may be used as a signature to identify true metformin hydrolases.

The recent spread of mfmA and mfmB genes across the world appears to be facilitated by horizontal gene transfer as the genes found in metformin-degrading Pseudomonas or Aminobacter species share >97% and >99% sequence identity at the protein and nucleotide level, respectively. In metformin-degrading Pseudomonas strains, mfmAB genes are located on plasmids while in Aminobacter genomes, the genes are either found on the main chromosome or on a plasmid (SI Appendix, Fig. S1). This suggests that MfmAB first evolved from an Aminobacter bacterium and the genes later moved into other *Pseudomonas* and *Aminobacter* strains on plasmids which contain transposon elements and type IV secretion systems (27).

Implications for Human Microbiomes. The identification of the metformin hydrolase enzyme in wastewater may have implications in metformin's interaction with human gut microbiota of type II diabetes patients. If MfmAB or an homologous enzyme exist in gut microbes then metformin metabolism may be occurring in the intestine and modulating the efficacy of the drug (10, 11). Another possibility is that gut enzymes, homologous to metformin hydrolase, may be inhibited by metformin which can compete with their native substrates. One homolog of MfmAB that is present in the human gut is agmatinase which acts on agmatine, an intermediate in polyamine metabolism (46). Interestingly, metformin and agmatine have been linked in a previous mechanistic study of metformin's effect on aging using a host-microbe system with C. elegans as the host and E. coli as the gut endosymbiont (47). E. coli encodes agmatinase, and a deletion of this gene done in the study simulated metformin's positive effect (47). Testing for metformin activity or inhibition of gut ureohydrolase homologs of metformin hydrolase may be important and merits further investigation.

Catalytic Mechanism of MfmAB. The catalytic mechanism of metformin hydrolysis by MfmAB appears similar to other members of the ureohydrolase superfamily in that it has the critical aspartate residue (D188) that is in close proximity to the water bound by the binuclear metals (Fig. 3D). The role of the asparate residue is to activate the water molecule and bind one of the metals (37). Substituting this residue with asparagine (D188N) was highly deleterious to specific activity which could support its role in catalysis but it also may affect binding of one of the binuclear metals as evidenced in the crystal structure of the D188N variant (PDB 8SNK), where one of the two metals is missing (SI Appendix, Fig. S7). In a previous study, the corresponding mutation was done in the E. coli agmatinase, D153N, and it was reported that the K_M for the native substrate, agmatine, was unchanged but with a 95% reduction of the specific activity (37).

A histidine residue that is present in the active sites of arginase, agmatinase, and guanidinium hydrolase, and is implicated in proton transfer to the amine leaving group on the substrate, is not present in MfmAB (36, 41). In MfmAB, the corresponding residue is an asparagine (N200), in which the side chain is not ionizable and likely has a role in substrate binding and/or transition state stabilization but not able to do proton transfer (Fig. 3D). A cysteine residue, C201, also in the active site, may be ionizable at the pH optimum of the enzyme, pH 9, but substitution of this residue with serine (C201S) did not dramatically affect the activity of the enzyme (Fig. 3D). The proton transfer to promote the elimination of dimethylamine from metformin may be facilitated by the catalytic aspartate, D188, which may transfer the proton it abstracts from the substrate-attacking water molecule to metformin (SI Appendix, Fig. S11). The docking model shows that for metformin to bind in a catalytic conformation, it may require that the substrate is contorted and not planar (Fig. 3*E*). This conformation could be stabilized by the active site residues (N200, E321, and D188) and by the two metals binding the substrate which could serve to reduce the resonance stabilization (Fig. 3D). The loss of planarity of amides is known to increase their lability in hydrolysis reactions, and this may also apply in the metformin hydrolysis catalyzed by MfmAB (48, 49).

Metal Dependency of MfmAB. The activity of metformin hydrolase is highest with divalent nickel compared to the other metals tested (Fig. 2B). Nickel is also the preferred metal for the enzymatic hydrolysis of urea and guanidine, which are both resonance stabilized structures, like metformin, and have higher activation barriers for hydrolysis compared to substituted guanidines, arginine, and agmatine, whose enzymes prefer divalent manganese (38). The greater Lewis acidity of nickel compared to manganese may be necessary to drive metformin and guanidine hydrolysis by further activating the metal-bound hydroxide that attacks the substrate. In addition, interactions with the substrate and geometry may also play a role in MfmAB's preference for nickel.

The delivery of nickel in vivo, into MfmAB, appears to be dependent on the coexpressed nickel-delivery proteins HypA and HypB. This is also likely the case for guanidinium hydrolase (GdmH) that has proteins GhaA and GhaB that are homologous to HypA and HypB (34). In the Irving-Williams series of divalent metals forming stable ligand complexes (ex. with proteins), only copper and zinc, which inhibit metformin hydrolase, are more competitive than nickel to form more stable complexes (Mn²⁺ < $Fe^{2+} < Co^{2+} < Ni^{2+} < Cu^{2+} > Zn^{2+}$) (50). This property of nickel then necessitates that its delivery must be facilitated in vivo to avoid mismetallation. So the likely role of the HypAB chaperones is to selectively deliver nickel to MfmAB in vivo where the endogenous concentration of nickel is at low levels compared to metals such as manganese and iron (51-53).

Materials and Methods

Cloning, Expression, and Purification of MfmAB. The metformin hydrolase genes, mfmA and mfmB from Pseudomonas mendocina sp. MET-2 (NCBI accessions WP_254300333.1 and WP_254300332.1, respectively), were codonoptimized and cloned into E. coli DH5 α cells (New England Biolabs) using a pETDuet vector derivative with kanamycin resistance (SI Appendix, Fig. S12). The mfmA gene was cloned with a C-terminal Tobacco Etch Virus (TEV) protease cleavage site followed by a 6×His-tag and inserted, by Gibson assembly, into the first multiple cloning site (MCS1) using the Ncol and HindIII restriction sites. The mfmB gene was not tagged and inserted into the second multiple cloning site (MCS2) using the Ndel and Xhol restriction sites. Site-directed mutants were made using the Q5 Site Directed Mutagenesis Kit from New England Biolabs. The vector containing the mfmAB genes was transformed into BL21 DE3 cells (New England Biolabs), and the proteins were expressed by growing cells in terrific broth (TB) medium supplemented with 0.5 mM NiSO₄ and 50 μg/mL kanamycin at 37 °C and 200 rpm to an OD_{600} of 0.6 in a shake flask. The culture was cooled to 16 °C and induced with 1 mM isopropyl β -D-1-thiogalactopyranoside (IPTG) and, with the same agitation, incubated for 20 h. Cell pellets were harvested by centrifugation at 1,500 \times g for 20 min and then resuspended in lysis buffer (50 mM Tris-HCl, 500 mM NaCl, and 10 mM 2-mercaptoethanol, pH 7.4). The cells were lysed using a French Press with three passes at 10,000 psi, and the lysate was then clarified by centrifugation at 20,000 \times g for 1 h. Metformin hydrolase was purified from the lysate by using fast protein liquid chromatography (FPLC) and immobilized metal affinity chromatography (IMAC). Using a GE-AKTA FPLC and a GE HisTrap 5 mL column, MfmAB was purified after running an imidazole gradient from

50 mM to 500 mM, and fractions were collected. The expression yield for MfmAB was 16 mg protein per liter culture. MfmAB protein concentrations were measured using the Bradford reagent with bovine serum albumin standards. Pooled fractions from the FPLC were buffer exchanged into storage buffer (20 mM HEPES-NaOH and 200 mM NaCl pH 8) using a 15-mL Amicon 10 kDa centrifugal filter. The His-tag of purified MfmAB was cleaved by adding 1 mg TEV protease in a dilute protein solution between 5 and 10 mg/mL MfmAB, and the cleavage reaction was placed on a rotator at 4 °C overnight. The reaction was concentrated to 2 mL, and cleaved MfmAB was purified by size-exclusion chromatography using the AKTA FPLC and a GE Healthcare HiLoad 16/600 Superdex 200 pg column. The column was equilibrated with storage buffer; the sample was injected onto the column and washed with 1 column volume at 1 mL per min flow rate. MfmAB eluted as a heterotrimer with an apparent molecular weight of ~180 kDa, and the preparation was then subsequently used in crystallization experiments (SI Appendix, Fig. S13). For metal reconstitution experiments, MfmAB enzyme was stripped of metal by incubating the enzyme with 1 mM 1,10-phenanthroline and 2.5 mM EDTA in storage buffer for 1 h before buffer exchanging the stripped enzyme into storage buffer using size-exclusion chromatography as described before.

Enzyme Activation and Kinetics. Rates of substrate hydrolysis by MfmAB were determined by a spectrophotometric, coupled-enzyme assay or by an HPLC method. Prior to enzyme kinetic assays, MfmAB was preincubated with 1 mM NiCl₂ in storage buffer on ice for 2 h to allow for complete activation of the enzyme. The coupled-enzyme assay included coupling of enzymes quanylurea hydrolase (GuuH) from Pseudomonas mendocina sp. MET-1 and bovine liver L-Glutamic dehydrogenase (GDH) with MfmAB to measure NADH oxidation that was proportional to guanylurea release from MfmAB (SI Appendix, Fig. S5). Guanylurea hydrolysis, via GuuH, generates guanidinium and ammonia which the latter can be used in reductive amination of 2-oxoglutarate to form L-glutamate, causing NADH oxidation that can be measured by absorbance at 340 nm. For reactions, a 10 × coupled enzyme assay master mix was prepared in 50 mM HEPES-NaOH pH 8 which had the following components and final concentrations: 0.3 mM NADH disodium salt (Sigma), 5 mM 2-oxoglutarate sodium salt (Aldrich), 0.8 mM adenosine diphosphate sodium salt (Sigma), 2.5 U/mL GDH from lyophilized powder (Sigma), and 0.3 mg/mL purified GuuH. Methods for expression and purification of GuuH are detailed by Martinez-Vaz et al. (27). The master mix was then diluted with buffer and purified MfmAB enzyme into wells of 96-well flat-bottom microplates, and the reaction was initiated by adding substrate to make a total sample volume of 200 µL. The reactions were monitored, continuously, by absorbance at 340 nm using an Agilent BioTek Synergy HTX microplate reader, and initial rates were recorded. Rates of NADH oxidation were calculated using the molar extinction coefficient for NADH, at 340 nm, of 6,220 M⁻¹cm⁻¹ and the pathlength of the assay volume (200 μ L) in the microplates, 0.56 cm. MfmAB enzyme concentrations used in the assay were between 0.01 μ g/mL and 12 μ g/mL to measure substrate hydrolysis with the rate being linearly dependent to enzyme concentration in this range (SI Appendix, Fig. S5). Negative controls for the assays included noenzyme and enzyme with no substrate that were used to measure background oxidation of NADH in the assay over time. Glycerol and Tris were found to inhibit MfmAB and were not used in enzyme kinetic assays. Guanylurea release was determined to be stoichiometric to NADH oxidation, and this was validated by an HPLC method that could separate and quantify metformin and guanylurea (SI Appendix, Fig. S5).

A reversed-phase HPLC method to separate guanylurea from metformin was adapted from Lin et al. and detailed by Martinez-Vaz et al. which, in brief, used a C18 column and an isocratic mobile phase of 75:25 (v/v) acetonitrile:10 mM potassium phosphate buffer pH 6.6 (27, 54). Kinetics were determined by incubating MfmAB with metformin in buffer, and aliquots were guenched with 75% (v/v) acetonitrile to take fixed time point measurements of the reaction. Quenched samples were injected onto the HPLC, and using standard curves, the concentrations of metformin and guanylurea were determined, based on the peak area at their respective λ_{max} , 234 nm and 220 nm, respectively. Rates of metformin consumption and guanylurea formation were determined using this HPLC method and were similar to the coupled-enzyme assay (SI Appendix, Fig. S5). One unit of activity (U) was defined as one micromole substrate per minute at the enzyme's pH optimum at 25 °C.

Substrates and NMR Spectroscopy. Metformin hydrochloride (Cayman Chemical), guanylurea phosphate (TCI Chemicals), dimethylamine hydrochloride (Acros), buformin hydrochloride (Enamine), phenformin hydrochloride (Cayman Chemical), biguanide hydrochloride (Synthonix), 1-methylbiguanide sulfate (Alfa), 1,1-dimethylguanidine hydrochloride (Aldrich), 1-methylguanidine hydrochloride (Aldrich), L-arginine hydrochloride (Acros), agmatine sulfate (Fluka), 4-guanidinobutyric acid (Fluka), and creatine hydrate (Sigma) were obtained with high purity (>97%). ¹H-NMR experiments were conducted in water with 20% D₂O using the Varian Unity Inova 400 MHz NMR system and VnmrQ 2.2 software. Sodium 3-(trimethylsilyl)-propionate-2,2,3,3-D4 salt (Cambridge Isotope Laboratories) was used as a reference standard.

Crystallization of MfmAB and Structure Elucidation. Initial crystallization conditions were found from the sparse matrix screen PACT Premier HT (Molecular Dimensions) using sitting drops containing 14 mg/mL MfmAB and reservoir solutions. Crystals grew from the following condition: 0.2 M NaNO $_3$, 0.1 M bis-tris propane, and 20% (w/v) PEG3350. Optimization of MfmAB crystals was done by vapor diffusion in 24-well hanging drop crystallization plates. Crystal growth was sensitive to changes to the relative humidity, and to prevent condensation, the air was purged from the wells with compressed nitrogen prior to sealing each well. Crystals grew in a range of conditions at 18 °C with 0.2 M NaNO $_3$ between 12 and 16% (w/v) PEG 3350 and 0.1 M bis-tris propane pH 7.5 to 8.5 in drops of 1 μ L of protein (5 to 10 mg/mL) with 1 or 2 μ L of precipitant. Crystals appeared after 1 d and were harvested by looping them into cryoprotectant [mother solution containing 25% (v/v) ethylene glycol] and frozen in liquid nitrogen.

Diffraction data were collected using the Advanced Photon Source (Argonne, Illinois, USA) with various beamlines (*SIAppendix*, Table S3). Data were processed using XDS (Build January 26, 2018) and molecular replacement; refinement was done using Molrep and Refmac within CCP4 (Version 7.0) and Coot (v0.8.9) (55–59). For the molecular replacement which was done similarly by a case study described by McCoy et al. (60), two separate models from the AlphaFold database were used (both 93% seq. id.), A0A2SOXPN7 and A0A316GGX0, to model MfmA and MfmB, respectively (61). The molecular replacement of the MfmAB complex proceeded by first placing monomers of MfmB into the asymmetric unit followed by deleting the monomers that poorly fit the electron density map upon inspection. The resulting solution was used as a fixed model to place monomers of MfmA, by molecular replacement, which was again inspected and, after a few more iterations, produced the final model that contained multiple copies of the MfmAB complex.

Computational Modeling and Bioinformatics. Docking metformin into the active site of MfmA was done using AutoDock Vina (Version 1.2.5), and ligand restraints were obtained from the ZINC20 database (ZINC12859773,

- P. M. Bradley et al., Metformin and other pharmaceuticals widespread in wadeable streams of the southeastern United States. Environ. Sci. Technol. Lett. 3, 243-249 (2016).
- J. L. Wilkinson et al., Pharmaceutical pollution of the world's rivers. Proc. Natl. Acad. Sci. U.S.A. 119, e2113947119 (2022).
- S. Amin, A. Lux, F. O'Callaghan, The journey of metformin from glycaemic control to mTOR inhibition and the suppression of tumour growth. Br. J. Clin. Pharmacol. 85, 37–46 (2019).
- K. Forslund et al., Disentangling type 2 diabetes and metformin treatment signatures in the human gut microbiota. Nature 545, 116 (2015).
- N. Tobar et al., Metformin acts in the gut and induces gut-liver crosstalk. Proc. Natl. Acad. Sci. U.S.A. 120, e2211933120 (2023).
- L. He, F. E. Wondisford, Metformin action: Concentrations matter. Cell Metab. 21, 159–162 (2015).
- M. Foretz, B. Guigas, B. Viollet, Metformin: Update on mechanisms of action and repurposing potential. Nat. Rev. Endocrinol. 19, 460-476 (2023).
- C. F. Sum et al., The effect of intravenous metformin on glucose metabolism during hyperglycaemia in type 2 diabetes. Diabet. Med. 9, 61–65 (1992).
- T. S. B. Schmidt, J. Raes, P. Bork, The human gut microbiome: From association to modulation. *Cell* 172, 1198–1215 (2018).
 M. A. Beliaeva, M. Wilmanns, M. Zimmermann, Decipher enzymes from human microbiota for drug
- discovery and development. *Curr. Opin. Struct. Biol.* **80**, 102567 (2023).

 11. M. Zimmermann, K. R. Patil, A. Typas, L. Maier, Towards a mechanistic understanding of reciprocal
- drug-microbiome interactions. *Mol. Syst. Biol.* **17**, e10116 (2021).

 12. G. Tucker *et al.*, Metformin kinetics in healthy subjects and in patients with diabetes mellitus.
- Br. J. Clin. Pharmacol. 12, 235-246 (1981).

 13. C. R. Sirtori et al., Disposition of metformin (N, N-dimethylbiguanide) in man. Clin. Pharmacol. Ther.
- C. R. Sirtori et al., Disposition of metformin (N, N-dimethylbiguanide) in man. Clin. Pharmacol. Thei 24, 683–693 (1978).
- G. T. Tucker, C. A. Wesolowski, Metformin disposition—A 40-year-old mystery. Br. J. Clin. Pharmacol. 86, 1452–1453 (2020).

https://zinc.docking.org/) (62, 63). The protein receptor was prepared using AutoDockTools4 (Version 4.2.6) with polar hydrogens added, using default charges for standard residues and the partial charges for nickel ions were set to 0.660 according to Sindhikara et al. (64, 65). The docking was done using the AutoDock4 forcefield with default parameters except the exhaustiveness was set to 100 and the ligand guanidinium torsions were set to rotatable. The top 10 binding modes shared an AutoDock score of -5.3, and the thirdbest binding mode is shown in Fig. 3 D and E. Homologous MfmA and MfmB sequences were mined from the NCBI and EMBL databases by first generating a sequence similarity network (SSN) using the EFI-EST tool that performed pairwise BLAST comparisons on 10,000 related sequences (66). Cytoscape was used to visualize the clustering in the SSN and identify the clusters containing MfmA and MfmB sequences (67).

Metal Content Analysis of MfmAB Using ICP-OES. A sample of 10 mg of MfmAB was buffer exchanged into 20 mM HEPES-NaOH pH 8 using a centrifugal filter and digested overnight with 5% (v/v) nitric acid (trace metals grade, Sigma). The digested sample was heated to 95 °C for 1 h, and then, the sample was clarified by centrifugation and the supernatant was collected and sent for analysis. A blank sample was prepared by using the flow-through from the centrifugal filter after buffer exchange and following the same procedure. Samples were sent to the Research Analytical Laboratory at the University of Minnesota for analysis using an iCap 7600 Duo ICP-OES Analyzer for inductively coupled plasma-optical emission spectroscopy (ICP-OES).

Data, Materials, and Software Availability. X-ray structures data have been deposited in RCSB (8SNF, 8SNK, and 8SP2) (68–70). All other data are included in the manuscript and/or *SI Appendix*.

ACKNOWLEDGMENTS. We thank Ke Shi from the Nanoliter Crystallization Facility at the University of Minnesota for initial crystal screening and beamline use to obtain diffraction data for the MfmAB apo structure. Jack Richman was instrumental in designing and conducting the NMR experiments. Sudipta Shaw is acknowledged for his expert advice on X-ray diffraction data collection, processing, and structure solution. Anna Saboe is thanked for her assistance in the site-directed mutagenesis experiments. Anthony Dodge is indebted to for his consultation on the experimental design and the manuscript. This research used resources of the Advanced Photon Source, a US Department of Energy (DOE) Office of Science user facility operated for the DOE Office of Science by Argonne National Laboratory under Contract No. DE-AC02-06CH11357. This work was supported by funding from the NSF (Grant no. 2203750), and L.J.T. was supported by a fellowship from the University of Minnesota Informatics Institute and Minnesota's Discovery, Research, and Innovation Economy (UMII-MnDRIVE).

- R. Q. Gabr, A. A. El-Sherbeni, M. Ben-Eltriki, A. O. El-Kadi, D. R. Brocks, Pharmacokinetics of metformin in the rat: Assessment of the effect of hyperlipidemia and evidence for its metabolism to guanylurea. Can. J. Physiol. Pharmacol. 95, 530-538 (2017).
- M. Scheurer, A. Michel, H. J. Brauch, W. Ruck, F. Sacher, Occurrence and fate of the antidiabetic drug metformin and its metabolite guanylurea in the environment and during drinking water treatment. Water Res. 46, 4790–4802 (2012).
- O. Golovko et al., Occurrence and removal of chemicals of emerging concern in wastewater treatment plants and their impact on receiving water systems. Sci. Total Environ. 754, 142122 (2021)
- M. Scheurer, F. Sacher, H. J. Brauch, Occurrence of the antidiabetic drug metformin in sewage and surface waters in Germany. J. Environ. Monit. 11, 1608–1613 (2009).
- C. Trautwein, J. D. Berset, H. Wolschke, K. Kümmerer, Occurrence of the antidiabetic drug Metformin and its ultimate transformation product Guanylurea in several compartments of the aquatic cycle. Environ. Int. 70, 203–212 (2014).
- J. O. Straub et al., Environmental risk assessment of metformin and its transformation product guanylurea. I. Environmental fate. Chemosphere 216, 844–854 (2019).
- S. Barros et al., Are fish populations at risk? Metformin disrupts zebrafish development and reproductive processes at chronic environmentally relevant concentrations. Environ. Sci. Technol. 57 (2022)
- G. A. Élizalde-Velázquez, S. E. Herrera-Vázquez, L. M. Gómez-Oliván, S. García-Medina, Health impact assessment after Danio rerio long-term exposure to environmentally relevant concentrations of metformin and guanylurea. *Chemosphere* 341 (2023).
- R. Zhang et al., Metformin chlorination byproducts in drinking water exhibit marked toxicities of a
 potential health concern. Environ. Int. 146, 106244 (2021).
- Y. He, Y. Zhang, F. Ju, Metformin contamination in global waters: Biotic and abiotic transformation, byproduct generation and toxicity, and evaluation as a pharmaceutical indicator. *Environ. Sci. Technol.* 56, 13528–13545 (2022).
- D. Armbruster et al., Emerging nitrogenous disinfection byproducts: Transformation of the antidiabetic drug metformin during chlorine disinfection of water. Water Res. 79, 104–118 (2015).

- 26. B. A. J. Poursat et al., Biodegradation of metformin and its transformation product, guanylurea, by natural and exposed microbial communities. Ecotoxicol. Environ. Saf. 182, 109414 (2019).
- B. M. Martinez-Vaz et al., Wastewater bacteria remediating the pharmaceutical metformin: Genomes, plasmids and products. Front. Bioeng. Biotechnol. 10, 2291 (2022).
- P. Chaignaud et al., A methylotrophic bacterium growing with the antidiabetic drug metformin as its sole carbon, nitrogen and energy source. Microorganisms 10, 2302 (2022).
- T. Li, Z. J. Xu, N. Y. Zhou, Aerobic degradation of the antidiabetic drug metformin by Aminobacter sp. strain NyZ550. Environ. Sci. Technol. 57, 1510-1519 (2022).
- K. B. Hillmann, T. D. Niehaus, Genome sequences of two Pseudomonas isolates that can use metformin as the sole nitrogen source. Microbiol. Resour. Announc. 11, e00639-22 (2022).
- L. J. Tassoulas, A. Robinson, B. Martinez-Vaz, K. G. Aukema, L. P. Wackett, Filling in the gaps in metformin biodegradation: A new enzyme and a metabolic pathway for guanylurea. Appl. Environ. Microbiol. 87, 1-13 (2021).
- N. O. Schneider et al., Solving the conundrum: Widespread proteins annotated for urea metabolism in bacteria are carboxyguanidine deiminases mediating nitrogen assimilation from guanidine Biochemistry 59, 3258-3270 (2020).
- C. O'Fágáin, P. M. Cummins, B. F. O'Connor, Gel-filtration chromatography. Methods Mol. Biol. 681, 33 15-25 (2011)
- D. Funck et al., Discovery of a Ni2+-dependent guanidine hydrolase in bacteria. Nature 603,
- A. Sekowska, A. Danchin, J. L. Risler, Phylogeny of related functions: The case of polyamine 35 biosynthetic enzymes. Microbiology 146, 1815-1828 (2000).
- S. V. Khangulov, T. M. Sossong, D. E. Ash, G. C. Dismukes, L-Arginine binding to liver arginase requires proton transfer to gateway residue His141 and coordination of the guanidinium group to the dimanganese(II, II) center. Biochemistry 37, 8539-8550 (1998).
- M. Salas et al., Insights into the reaction mechanism of Escherichia coli agmatinase by site-directed mutagenesis and molecular modelling: A critical role for aspartate 153. Eur. J. Biochem. 269, 5522-5526 (2002).
- 38 C. A. Lewis, R. Wolfenden, The nonenzymatic decomposition of guanidines and amidines. J. Am. Chem. Soc. 136, 130-136 (2014).
- J. A. Hyung et al., Crystal structure of agmatinase reveals structural conservation and inhibition 39 mechanism of the ureohydrolase superfamily. J. Biol. Chem. 279, 50505-50513 (2004).
- 40 D. P. Dowling, L. Di Costanzo, H. A. Gennadios, D. W. Christianson, Evolution of the arginase fold and functional diversity. Cell. Mol. Life Sci. 65, 2039-2055 (2008).
- R. C. Cavalli, D. R. Soprano, D. E. Ash, C. J. Burke, S. Kawamoto, Mutagenesis of rat liver arginase expressed in Escherichia coli: Role of conserved histidines. Biochemistry 33, 10652-10657 (1994).
- N. Carvajal et al., Kinetic studies and site-directed mutagenesis of Escherichia coli agmatinase. A role for Glu274 in binding and correct positioning of the substrate quanidinium group. Arch. Biochem. Biophys. 430, 185-190 (2004).
- L. Di Costanzo et al., Crystal structure of human arginase I at 1.29-Å resolution and exploration of inhibition in the immune response. Proc. Natl. Acad. Sci. U.S.A. 102, 13058–13063 (2005).
- $A.\,Bar-Even\,\textit{et al.}, The\ moderately\ efficient\ enzyme:\ Evolutionary\ and\ physicochemical\ trends$ shaping enzyme parameters. Biochemistry 50, 4402-4410 (2011).
- M. Nattrass, K. G. M. M. Alberti, Biguanides. Diabetologia 14, 71–74 (1978).
- Y. Kitada et al., Bioactive polyamine production by a novel hybrid system comprising multiple indigenous gut bacterial strategies. Sci. Adv. 4, 62-89 (2018).
- R. Pryor et al., Host-microbe-drug-nutrient screen identifies bacterial effectors of metformin therapy. Cell 178, 1299-1312.e29 (2019).
- D. A. O. G. De Velasco et al., Unexpected resistance to base-catalyzed hydrolysis of nitrogen pyramidal amides based on the 7-azabicyclic[2.2.1]heptane scaffold. Molecules 23, 2363 (2018).

- 49. S. Yamada, Structure and reactivity of a highly twisted amide. Angew. Chem. Int. Ed. English 32, 1083-1085 (1993)
- H. Irving, R. J. P. Williams, Order of stability of metal complexes. *Nature* **162**, 746–747 (1948).

 A. M. Sydor, H. Lebrette, R. Ariyakumaran, C. Cavazza, D. B. Zamble, Relationship between Ni(II) and Zn(II) coordination and nucleotide binding by the helicobacter pylori [NiFe]-hydrogenase and urease maturation factor HypB. J. Biol. Chem. 289, 3828-3841 (2014).
- 52. H. Kaluarachchi, K. C. Chan Chung, D. B. Zamble, Microbial nickel proteins. Nat. Prod. Rep. 27, 681-694 (2010).
- K. A. Higgins, C. E. Carr, M. J. Maroney, Specific metal recognition in nickel trafficking. Biochemistry **51**, 7816–7832 (2012).
- M. C. Lin, J. H. Lin, K. C. Wen, Detection and determination of phenformin in chinese medicinal capsules by GC-MS and HPLC. J. Food Drug Anal. 9, 139–144 (2001).
- W. Kabsch, Automatic processing of rotation diffraction data from crystals of initially unknown symmetry land cell constants. J. Appl. Crystallogr. 26, 795-800 (1993).
- P. Emsley, K. Cowtan, Coot: Model-building tools for molecular graphics. Acta Crystallogr. Sect. D Biol. Crystallogr. 60, 2126-2132 (2004).
- A. Vagin, A. Teplyakov, MOLREP: An automated program for molecular replacement. J. Appl. Crystallogr. 30, 1022-1025 (1997).
- M. D. Winn, M. N. Isupov, G. N. Murshudov, Use of TLS parameters to model anisotropic displacements in macromolecular refinement. Acta Crystallogr. Sect. D Biol. Crystallogr. 57, 122-133
- G. N. Murshudov et al., REFMAC5 for the refinement of macromolecular crystal structures. Acta Crystallogr. Sect. D Biol. Crystallogr. 67, 355-367 (2011).
- A. J. McCoy, Solving structures of protein complexes by molecular replacement with Phaser. Acta Crystallogr. D Biol. Crystallogr. 63, 32-41 (2006).
- J. Jumper et al., Highly accurate protein structure prediction with AlphaFold. Nature 596, 583-589
- J. J. Irwin et al., ZINC20 A free ultralarge-scale chemical database for ligand discovery. J. Chem. Inf. Model. 60, 6065-6073 (2020).
- J. Eberhardt, D. Santos-Martins, A. F. Tillack, S. Forli, AutoDock Vina 1.2.0: New docking methods, expanded force field, and Python bindings. J. Chem. Inf. Model. 61, 3891–3898 (2021).
- D. J. Sindhikara, A. E. Roitberg, K. M. Merz, Apo and nickel-bound norms of the Pyrococcus horikoshii species of the metalloregulatory protein: NikR characterized by molecular dynamics simulations. Biochemistry 48, 12024-12033 (2009).
- G. M. Morris et al., AutoDock4 and AutoDockTools4: Automated docking with selective receptor flexibility. J. Comput. Chem. 30, 2785-2791 (2009).
- J. A. Gerlt et al., Enzyme function initiative-enzyme similarity tool (EFI-EST): A web tool for generating protein sequence similarity networks. Biochim. Biophys. Acta-Proteins Proteomics 1854, 1019-1037 (2015).
- P. Shannon et al., Cytoscape: A software environment for integrated models of biomolecular interaction networks. Genome Res. 13, 2498-2504 (2003).
- L. J. Tassoulas, J. A. Rankin, M. H. Elias, L. P. Wackett, Crystal structure of metformin hydrolase (MfmAB) from Pseudomonas mendocina sp. MET-2 with Ni2+2 bound. Protein Data Bank. https:// www.rcsb.org/structure/8SNF. Deposited 27 April 2023.
- L. J. Tassoulas, J. A. Rankin, M. H. Elias, L. P. Wackett, Crystal structure of metformin hydrolase (MfmAB) from Pseudomonas mendocina sp. MET-2 mutant (MfmA/D188N). Protein Data Bank. https://www.rcsb.org/structure/8SNK. Deposited 27 April 2023.
- L. J. Tassoulas, J. A. Rankin, M. H. Elias, L. P. Wackett, Crystal structure of metformin hydrolase (MfmAB) from Pseudomonas mendocina sp. MET-2 apo form. Protein Data Bank. https://www.rcsb. org/structure/8SP2. Deposited 1 May 2023.